Numerical Study on the Velocity Structure around Tidal Fronts in the Yellow Sea

LIU Guimei*[1,2] (刘桂梅), WANG Hui[3] (王 辉), SUN Song[1] (孙 松), and HAN Boping[1] (韩博平)

[1] *Key Laboratory of Marine Ecology and Environmental Sciences, Institute of Oceanology, Chinese Academy of Sciences, Qingdao* 266071

[2] *ICCES, Institute of Atmospheric Physics, Chinese Academy of Sciences, Beijing* 100029

[3] *National Natural Science Foundation of China, Beijing* 100085

(Received April 1, 2002; revised February 24, 2003)

ABSTRACT

The velocity components across tidal fronts are examined using the Blumberg and Mellor 3-D nonlinear numerical coastal circulation model incorporated with the Mellor and Yamada level 2.5 turbulent closure model based on the reasonable model output of the M_2 tide and density residual currents. In the numerical experiments, upwelling motion appears around all the fronts with different velocity structures, accounting for surface cold water around the fronts. The experiments also suggest that the location and formation of fronts are closely related to topography and tidal mixing, as is the velocity structure around the front.

Key words: 3-D velocity around tidal fronts, tidal mixing, topography

1. Introduction

The Yellow Sea is a large, partly closed sea with average water depth of 44 m (Fig.1), and has large tidal ranges and strong semidiurnal tidal currents due to its basin geometry and topography (Zhao et al., 1994; Wan et al., 1998; Wang et al., 1999; Sun et al., 2001). The continental tidal mixing front identified by satellite images of the sea surface temperature is considered to control the boundary of the summer Yellow Sea Cold Water Mass (YSCWM) (Zhao, 1985, 1987a, b). The formation of the tidal front is mainly associated with large tidal energy, prominent seasonal temperature variation, and lower residual currents (Zhao, 1987a).

Although previous studies on the tidal fronts in the Yellow Sea have provided useful information based on the observed data, satellite image analysis (Zhao, 1985, 1987a, b; Tang and Zheng, 1990), and numerical studies (Bi and Zhao, 1993; Qi and Su, 1998), the models used in the numerical studies are two-dimensional (2-D) or simple three-dimensional (3-D) models treating salinity as a constant. Therefore, the horizontal and vertical circulation structures around the tidal front are not clearly simulated. Further investigation is necessary in order to understand the impact of circulation around the tidal fronts on the plankton (Liu et al., 2002). To gain 3-D information, a 3-D baroclinic turbulent closure model is applied to the study of the tidal front and its circulation structure in this paper.

2. Numerical model

The model used in this study is the combination of the Blumberg and Mellor (1987) 3-D nonlinear coastal

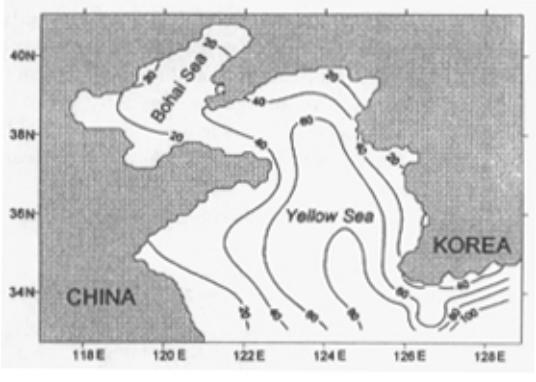

Fig. 1. The water depth of the Bohai Sea and Yellow Sea.

*E-mail: liuguimei@ms.qdio.ac.cn

circulation model and the Mellor and Yamada (1974, 1982) level 2.5 turbulent closure model so it can provide a realistic parameterization for the coastal vertical mixing and circulation. The equations considered in the 3-D coastal ocean circulation model are:

$$\frac{\partial u}{\partial t}+u\frac{\partial u}{\partial x}+v\frac{\partial u}{\partial y}+w\frac{\partial u}{\partial z}-fv = -\frac{1}{\rho_o}\frac{\partial P}{\partial x}+\frac{\partial}{\partial z}\left(K_m\frac{\partial u}{\partial z}\right)+F_u, \quad (1)$$

$$\frac{\partial v}{\partial t}+u\frac{\partial v}{\partial x}+v\frac{\partial v}{\partial y}+w\frac{\partial v}{\partial z}+fu = -\frac{1}{\rho_o}\frac{\partial P}{\partial y}+\frac{\partial}{\partial z}\left(K_m\frac{\partial v}{\partial z}\right)+F_v, \quad (2)$$

$$\frac{\partial P}{\partial z}=-\rho g, \quad (3)$$

$$\frac{\partial u}{\partial x}+\frac{\partial v}{\partial y}+\frac{\partial w}{\partial z}=0, \quad (4)$$

$$\frac{\partial \theta}{\partial t}+u\frac{\partial \theta}{\partial x}+v\frac{\partial \theta}{\partial y}+w\frac{\partial \theta}{\partial z} = \frac{\partial}{\partial z}\left(K_h\frac{\partial \theta}{\partial z}\right)+F_\theta, \quad (5)$$

$$\frac{\partial s}{\partial t}+u\frac{\partial s}{\partial x}+v\frac{\partial s}{\partial y}+w\frac{\partial s}{\partial z} = \frac{\partial}{\partial z}\left(K_h\frac{\partial s}{\partial z}\right)+F_s \quad (6)$$

$$\rho=\rho(\theta,s), \quad (7)$$

where (x, y, z) and (u, v,w) are respectively the Cartesian coordinates and corresponding velocity components with easterly, northerly, and upward as positive u, v, and w; θ the potential temperature; s the salinity; ρ the density; P the pressure; f the Coriolis parameter; g the gravitational acceleration; K_m the vertical eddy viscosity coefficient; and K_h the thermal vertical eddy friction coefficient. F_u, F_v, F_θ, and F_s represent the horizontal momentum, thermal, and salinity diffusion terms respectively. Adopting the level 2.5 (MY-2.5) turbulent closure scheme (Mellor and Yamada, 1982) modified by Galperin et al. (1988), K_m and K_h can be parameterized.

The surface and bottom boundary conditions are:

$$z=\zeta(x,y,t),\quad \frac{\partial\theta}{\partial z}=\frac{\partial s}{\partial z}=0,$$
$$w=\frac{\partial\zeta}{\partial t}+u\frac{\partial\zeta}{\partial x}+v\frac{\partial\zeta}{\partial y},$$
$$K_m\left(\frac{\partial u}{\partial z},\frac{\partial v}{\partial z}\right)=(0.,0.),$$

$$z=-H(x,y),\quad \frac{\partial\theta}{\partial z}=\frac{\partial s}{\partial z}=0,$$
$$w=-u\frac{\partial H}{\partial x}-v\frac{\partial H}{\partial y},$$
$$K_m\left(\frac{\partial u}{\partial z},\frac{\partial v}{\partial z}\right)=\frac{1}{\rho_0}\left(\tau_{bx},\tau_{by}\right),$$

where H is the mean water depth, ζ the free surface elevation, $(\tau_{bx},\tau_{by})=C_d\sqrt{u^2+v^2}\,(u,v)$ the x and y components of bottom stresses respectively, and C_d the drag coefficient with value of 0.001 in the Bohai Sea and 0.0018 in the Yellow Sea. The σ-coordinate transformation $\sigma=(z-\zeta)/(H+\zeta)$ is used to handle the irregular topography. With solid boundaries, the velocity component normal to the boundary must be zero, that is $v_n=0$.

The semi-implicit numerical scheme "ECOM-si" (Blumberg, 1992) is adopted to treat implicitly the barotropic pressure gradient in the momentum equations and the barotropic velocity divergence in the continuity equation. This leads to a linear, symmetrical, five diagonal system for water surface elevation that can be solved efficiently by a preconditioned conjugate gradient method with no sacrifice in computation time (Casulli, 1990). The vertical friction terms are computed with an implicit numerical scheme while the horizontal advection terms are treated explicitly in the semi-implicit scheme. The model time step is 621 seconds (72 time steps over an M_2 tidal cycle). The accuracy of the numerical scheme is second order in time and space.

The considered region in our model is (33°-41°N, 117.5°-127°E) with 145×100 grid points and 5′ × 5′ as horizontal resolution. In the vertical resolution, 20 sigma levels are uniformly distributed in the water column with $\Delta\sigma=0.05$.

The model was forced initially by the barotropic mode with M_2 tidal amplitude and phase at the open boundary (south at 33°N and east at 127°E) according to the tidal chart in the *Marine Atlas* (Chen et al., 1992). After the barotropic model reaches steady state, the baroclinic terms (August climatological mean temperature and salinity) (Chen et al., 1992) were put into the model and run for 20 tidal cycles.

3. The model results

3.1 *Tidal model verification*

The model with homogeneous water reaches steady state in 5 tidal cycles. The analysis here is carried out for the 10th tidal period. Four amphidromic points can be identified in the 10th amplitude and phase field (Fig. 2) , which agree well with previous works (Fang,

1986; Zhao et al., 1994; Wan et al., 1998; Wang et al., 1999). The mean differences between model and observed M_2 tidal amplitude and phase are 4.6 cm and 3.9° (Table 1). Those results indicate that the model reproduces proper tidal currents.

The Eulerian tidal residual current is defined as the time average of the tidal velocity at each grid point over one tidal cycle. With only M_2 tidal forcing, the Eulerian tidal residual currents are well developed in the northern Yellow Sea, west coast of Korea, and Subei shallow water region (Fig. 3). The maximum velocity magnitude of 10 cm s^{-1} may be associated with the sharp changes of the coastline (Fang and Yang, 1985) or the bottom slope (Loder, 1980). Such tidal residual currents are similar to those provided by Zhao et al. (1995) and Lee and Beardsley (1999).

3.2 *The density residual currents*

In the case with the August climatological mean temperature and salinity as the initial conditions, the residual currents (Fig.4) are significantly increased in magnitude compared to the case with homogeneous water as initial condition (Fig. 3). Figure 4 shows a counter-clockwise circulation with northward flow along the 50 m isobath in the Yellow Sea, an eastward flow at about 36°N, and a southward flow along the west coastline of Korea. And at the east coast of the Shandong Peninsula (36°N) the currents are weak and broad and become narrow and strong at about 34.5°N. The magnitude of the residual currents is about 10 cm s^{-1} , but it almost reaches 20 cm s^{-1} at the east cape of the Shangdong Peninsula. Model and observational results agree well with each other (Zhao et al., 1991; Lin et al., 2002), indicating the density residual currents are robust and the baroclinity has an important impact on the summertime flow in the Yellow Sea.

3.3 *Vertical circulation structure around the tidal fronts*

From the temperature distribution at the bottom layer (Fig. 5), the front location can be identified along the west shore of the southern Yellow Sea, the southwest of Korea, the northern Yellow Sea, the cape at the east coast of the Shandong Peninsula, etc. A further investigation is carried out with a vertical cross-section along 36.9°N and 34.4°N.

3.3.1 The vertical cross section along 36.9°N

The temperature profile (Fig. 6a) shows that the tidal fronts are located at the western boundary around 122.9°N and at the eastern bottom slope around 125.5°N, and the water is well stratified between the fronts.

At the western boundary front, the vertical velocity w profile (Fig. 6c) shows downwelling at the bottom layer while upwelling at the upper layer, a divergence zone can be identified around the upper layer of the front according to the dipole in the u component field (Fig. 6b), and an axis of maximum v component extends from the surface to the deep region near the bottom slope and the value becomes smaller as the depth increases (Fig. 6d).

In the observed geostrophic velocity across the front at a similar section obtained by Zhao (1987a),

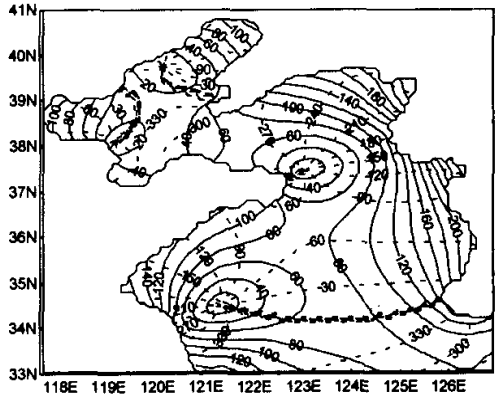

Fig. 2. Model-predicted co-amplitudes (solid, in cm) and co-phases (dashed, in degree) of the M_2 tide in Yellow Sea.

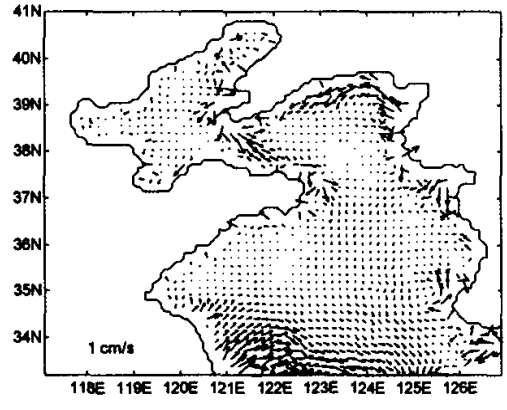

Fig. 3. The vertically-averaged tidal residual currents in the Yellow Sea with only M_2 tidal forcing.

a similar v profile was found, except its maximum v at the subsurface may be due to the simplification of the model.

At 125.5°E the upward motion also takes place around the bottom front and the downwelling takes place on both sides of the front (Fig. 6c). The diver-

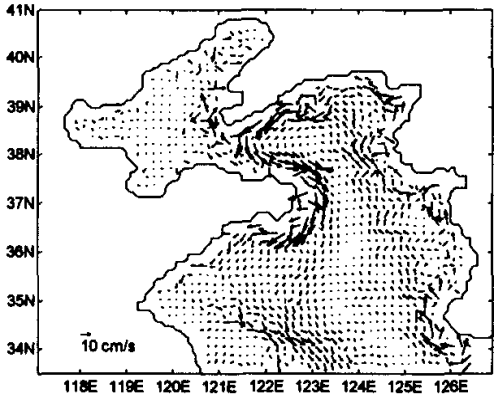

Fig. 4. The vertically averaged model predicted density residual currents in the Yellow Sea with August climatological mean temperature and salinity as initial conditions.

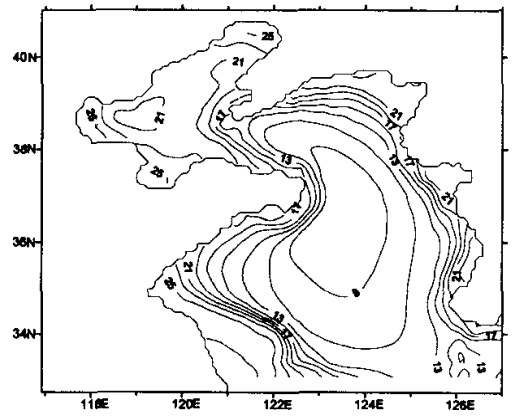

Fig. 5. The August climatological mean temperature (°C) at the bottom layer.

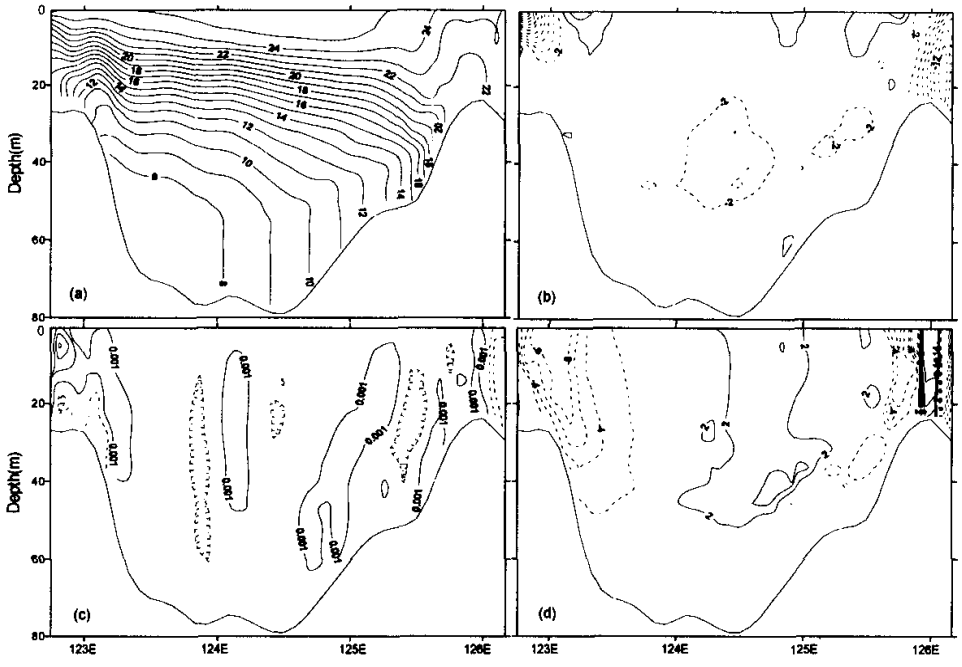

Fig. 6. The vertical cross section along 36.9°N for temperature (a, in °C), u component (b, positive for eastward), w component (c, positive for upward), v component (d, positive for northward) of residual currents (cm s^{-1}).

Table 1. Model-data comparison of the M_2 tidal amplitude and phase in the Yellow Sea

Longitude (°E)	Latitude (°N)	Amplitude (cm)		Phase (°)	
		Model	Observed	Model	Observed
123.2	39.1	123.2	126	246.6	249.7
122.7	39.3	134	124.9	260.3	261.3
122.2	40.6	124.5	123.9	133.7	144.3
121	40.7	87.9	95.5	151.9	150.5
119.6	39.9	16.7	10.7	316.9	313.4
121.5	36.8	122.5	112.7	88.5	88.6
124.4	39.7	209.8	206	242	239
124.3	39.8	203.6	212	243.5	246
123.1	39.5	154.6	158	252.2	254
125.6	37.7	196.6	198	127.3	120
126.6	37.5	295.3	293	123.3	113
126.1	36.8	219.6	220	86.8	84
The absolute mean differences		4.6		3.9	

gence zone is around 125.8°E according to the u component (Fig. 6b), and the v component is high at the divergence zone and the eastern solid boundary (Fig. 6d). The circulation structure around the front at 125.5°E agrees with the hypothesis provided by Zhao (1987a). Lough and Manning (2001) also found there was a two-cell circulation pattern with upwelling flow on the mixed side of the front and a surface convergence and downwelling on the stratified side across southern flank of Georges Bank in May 1997.

3.3.2 The vertical cross section along 34.4°N

The temperature profile along 34.4°N shows that there is a tidal front in the bottom layer from around 121.3°E to 122°E (Fig.7a). The vertical motion w is complicated (Fig. 7c), showing upwelling and downwelling intermittently around the front. The u component (Fig. 7b) is positive at the region and the maximum u can reach 8 cm s^{-1} at the top of the bottom

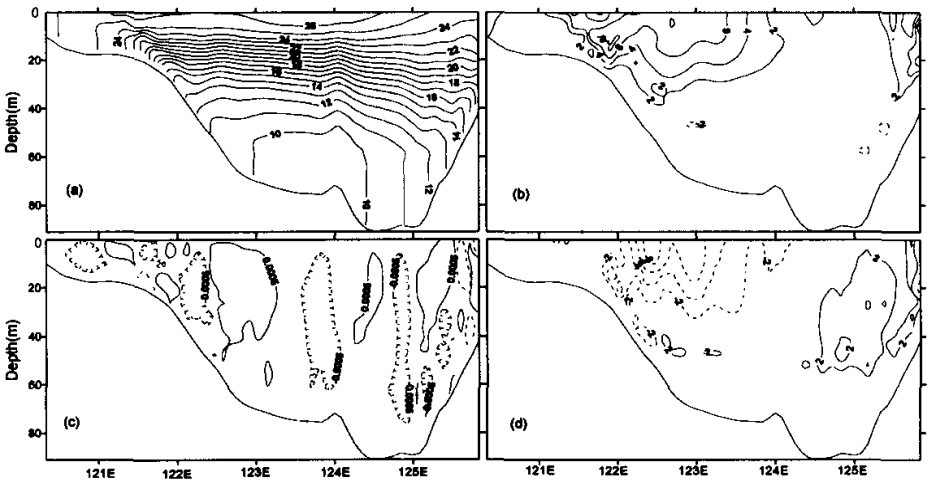

Fig. 7. The same as Fig. 6 except for along 34.4°N.

mixed layer in the frontal region. The magnitude and distribution of the v component is also similar to that obtained by Zhao (1987a) at another similar section, except that the observed maximum v appears in the middle layer at the bottom slope. These model results suggest that although the u, v and w components are quite different in different frontal conditions, upwelling appears in all cases, accounting for the surface cold water around the fronts (Zhao, 1987a). And the high horizontal velocity v component predicted at the front is agreed with by Chen and Beardsley (1995) and Lee and Beardsley (1999) who suggested the residual tidal currents at the fronts and at the top of the bottom mixed layer over the sloping bottom could be intensified. The simulation results not only agree with the numerical results of a 2-D model (Su and Huang, 1995; Bi and Zhao, 1993; Zhao, 1996), but also provide a better resolution for u across the fronts.

The following numerical experiments are designed to examine the role of the tidal force and topography in frontogenesis and the velocity structure around the fronts.

4. Numerical experiments

4.1 *Tidal forcing*

With initial conditions of a uniform horizontal temperature at each water depth, a linear decrease in temperature with increase of depth (Fig. 8), and a homogeneous salinity in the whole water column, the numerical results (after a steady state is reached) show that the tidal fronts (Fig. 9a) appear in the same region as those with the field climatological data (Fig. 5).

Figure 9b shows that off the Chinese and Korean coasts, the initial stratification (Fig. 8) is completely destroyed in the water shallower than 30 m, resulting

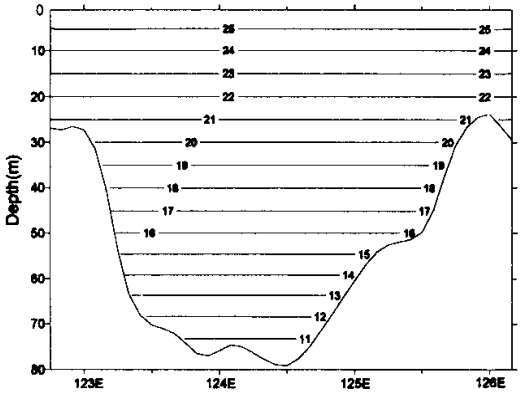

Fig. 8. The initial temperature profile at section 36.9°N for numerical experiment.

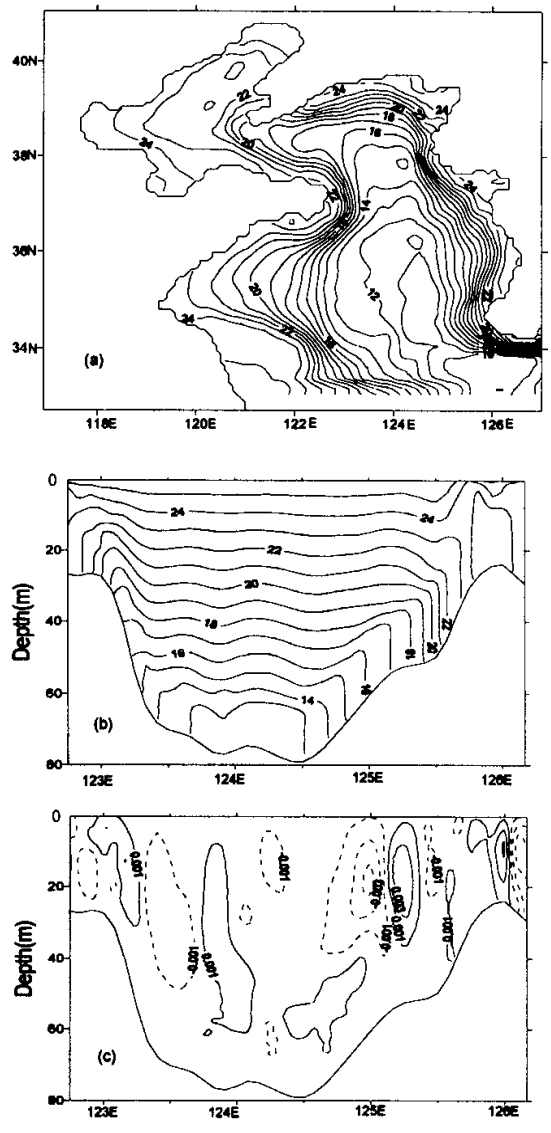

Fig. 9. (a) The temperature distribution (°C) at the bottom layer, (b) temperature profile and, (c) velocity w (cm s^{-1}) profile in the vertical cross section at 36.9°N with linear stratification after steady state is reached. The dotted lines stand for negative.

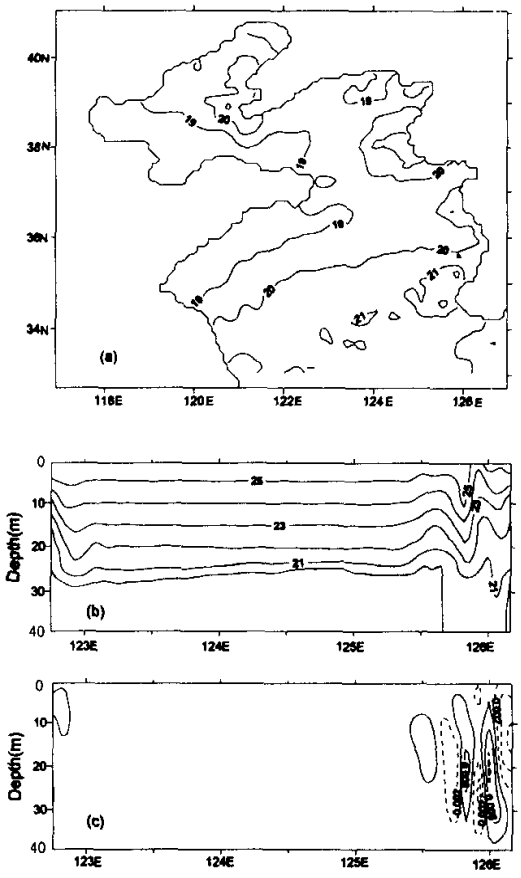

Fig. 10. The same as Fig. 9 except for a homogeneous water depth of 40 m.

in a locally homogeneous water column in these areas. In the central Yellow Sea, the stratification is still similar to the initial condition with little change in the tidal front's location (Fig. 9b and Fig. 6a). The distinct tidally-mixed bottom boundary layer has been established in 10 m of the bottom layer. The bottom mixed layer is thicker in the eastern than in the western part of the Yellow Sea, which may be due to the stronger tidal mixing in the eastern part. A slight change appears in the velocity component w (Fig. 9c). This experiment indicates the importance of tidal mixing in frontogenesis.

4.2 *The effect of topography*

With the same initial conditions as the linear stratification case, and a fixed water depth of 40 m for the whole region of study, the tidal fronts disappear from the bottom layer of the Yellow Sea (Fig. 10a), so does the front's cross section at 36.9°N after a steady state is reached. Strong upwelling and downwelling occur near the east boundary (Fig. 10c) due to the strong tidal force at the eastside, which is quite different from the result with real topography (Fig. 6c). This experiment reveals the important effect of the topography on the frontogenesis and the structure of velocity.

5. Conclusion

In the present numerical study, the tidal results and the density circulation magnitude and pattern are consistent with the observations, indicating a reasonably simulated vertical circulation structure around the fronts. Although the structures of velocity are quite different around different fronts, upwelling appears in all front conditions, accounting for the surface cold water around the fronts (Zhao, 1987a). The numerical experiments also suggest that the topography and tidal mixing play key roles in frontogenesis, in the location of the fronts, and in the velocity structure. Further study will focus on the dynamics controlling plankton distributions in the frontal region.

Acknowledgments. *This research was supported* by the Chinese Academy of Sciences (No. 131, 100 talents project), the National Key Fundamental Developing Project (No. G19990437-02, -08) and the National Natural Science Foundation of China (No. 49976032 and No. 49928605). The authors are grateful for the support of the Marine Department of the University of Georgia. Thanks also go to Prof. Zhao B.R. and the anonymous reviewers for their valuable comments.

REFERENCES

Bi Yawen, and Zhao Baoren, 1993: The numerical vertical structure simulation on the continental shelf front at southwest of the Yellow Sea. *Marine Science*, **6**, 61–63. (in Chinese)

Blumberg, A. F., and G. L. Mellor, 1987: A description of a three-dimensional coastal ocean circulation model. *Three-Dimensional Coastal Models*, Amer. Geophys. Union, 1–16.

Blumberg, A. F., 1992: *A primer for Ecom-si.* Technical Report, HydroQual, Inc., Mahwah, N. J., 64 pp.

Casulli, V., 1990: Semi-implicit finite-difference methods for the two-dimensional shallow water equations. *J. Comput. Phys.*, **86**, 56–74.

Chen, C., and R. C. Beardsley, 1995: A numerical study of stratified tidal rectification over finite-amplitude banks. Part I: Symmetric Banks. *Journal of Physical Oceanography*, **25**, 2090–2110.

Chen Guozhen, and Coauthors, 1992: *Marine Atlas of Bohai Sea, Huanghai Sea and East China Sea (Hydrology)*. China Ocean Press, Beijing. 432 pp. (in Chinese)

Fang Guohong, 1986: Tide and tidal current charts for the marginal seas adjacent to China. *Chin. J. of Oceanology and Limnology*, **4**(1), 337–345. (in Chinese)

Fang Guohong and Yang Jingming, 1985: A 2D numerical model on the simulation of the tide in the Bohai Sea. *Oceanologia et Limnologia Sinica*, **16**(5), 337–345. (in Chinese)

Galperin B., L. H. Kantha, S. Hassid, A. Rosati, 1988: A quasi-equilibrium turbulent energy model for geophysical flows. *J. Atmos. Sci.*, **45**, 55–62.

Lee Sang-Ho, and R. C. Beardsley, 1999: Influence of stratification on residual tidal currents in the Yellow Sea. *J. Geophys. Res.*, **104**(C7), 15679–15701.

Lin Kui, Tang Yuxiang, and Guo Binghuo, 2002: An analysis on observational surface and upper layer current in the Huanghai Sea and the East China Sea. *Acta Oceanologica Sinica*, **24**(2), 9–19. (in Chinese)

Liu Guimei, Sun Song, Wang Hui, and Liu Huilian, 2002: Influence of oceanic fronts on the *Calanus sinicus* in the Yellow Sea. *Progress in Natural Science*, **12**(11), 1150–1154. (in Chinese)

Loder, J. W., 1980: Topographic rectification of tidal currents on the sides of Georges Bank. *J. Phys. Oceanogr.*, **110**, 1399–1416.

Lough, R. G., and J. P. Manning, 2001: Tidal-front entrainment and retention of fish larvae on the southern flank of Georges Bank. *Deep-Sea Research II*, **48** (1-3), 631–644.

Mellor, G. L., and T. Yamada, 1974: A hierarchy of turbulence closure models for planetary boundary layers. *J. Atmos. Sci.*, **33**, 1791–1896.

Mellor, G. L., and T. Yamada, 1982: Development of a turbulence closure model for geophysical fluid problems. *Rev. Geophys. Space Phys.*, **20**, 851–875.

Qi Jianhua and Su Yusong, 1998: The numerical research on the tidal shelf front in the Yellow Sea. *Oceanologia et Limnologia Sinica*, **29**(3), 247–253. (in Chinese)

Su Jilan and Huang Daji, 1995: On the current field associated with the Yellow Sea Cold Water Mass. *Oceanologia et Limnologia Sinica Supplement*, **26**(5), 1–7. (in Chinese)

Sun Wenxin, Liu Guimei, Lei Kun, Jiang Wensheng, and Zhang P., 2001: A numerical study on circulation in the Yellow Sea and East China Sea II: Numerical simulation of tide and tide-induced circulation. *Journal of Ocean University of Qingdao*, **31**(3), 297–304. (in Chinese)

Tang Yuxiang, and Zheng Yifang, 1990: Research on fronts in the East China Sea. *Marine Science Bulletin*, **9**(5), 89–96. (in Chinese)

Wan Zhenwen, Qiao Fangli, and Yuan Yeli, 1998: Three-dimesional numerical modeling of tidal waves in the Bohai, Yellow and East China Seas. *Oceanologia et Limnologia Sinica*, **29**(6), 611–616. (in Chinese)

Wang Kai, Fang Guohong, and Feng Shizuo, 1999: A 3-D numerical simulation of M_2 tides and tidal currents in the Bohai Sea, the Huanghai Sea and the East China Sea. *Acta Oceanologica Sinica*, **21**(4), 1–13. (in Chinese)

Zhao Baoren, 1985: The fronts of the Huanghai Sea Cold Water Mass induced by tidal mixing. *Oceanologia et Limnologia Sinica*, **16**(6), 451–459. (in Chinese)

Zhao Baoren, 1987a: A preliminary study of continental shelf fronts in the western part of the southern Huanghai Sea and circulation structure in the front region of the Huanghai Cold Water Mass (HCWM). *Oceanologia et Limnologia Sinica*, **18**(3), 217–226. (in Chinese)

Zhao Baoren, 1987b: The continental shelf fronts induced by tidal mixing in the Huanghai Sea. *Journal of Oceanography of Huanghai & Bohai Seas*, **5**(2), 16–23. (in Chinese)

Zhao Baoren, 1996: A study of the circulations of the northern Yellow Sea Cold Water Mass—Effects of tidal mixing on them. *Oceanologia et Limnologia Sinica*, **27**(4), 429–435. (in Chinese)

Zhao Baoren, R. Limeberner, Hu Dunxin, and Cui Maochang, 1991: Oceanographic characteristics of the southern Yellow Sea and the northern East China Sea in summer. *Oceanologia et Limnologia Sinica*, **22**(2), 132–139. (in Chinese)

Zhao Baoren, Fang Guohong, and Cao Deming, 1994: Numerical simulation of tide and tidal currents in the Bohai, Yellow and East China Seas. *Acta Oceanologica Sinica*, **16**(5), 1–10.(in Chinese)

Zhao Baoren, Fang Guohong, and Cao Deming, 1995: Characteristics of tidal residual currents and their relations with coastal current transports in the Bohai Sea, Yellow Sea and East China Sea. *Studia Marina Sinica*, **36**, 1–11. (in Chinese)

黄海夏季潮汐锋区环流的数值研究

刘桂梅 王 辉 孙 松 韩博平

P7 A

摘 要

基于Blumberg & Mellor 三维非线性环流模型（ECOM）并结合Mellor & Yamada 的湍封闭模型，对黄海M_2分潮、密度环流、锋区环流等进行了的数值模拟：潮汐模拟结果较好的体现了黄、渤海M_2潮波传播系统，验证了模型的可行性；模拟密度环流的量阶和方向均与夏季实测环流保持一致，体现了密度环流是夏季总环流的重要组成部分；两个断面锋区环流的模拟结果显示锋区位置不同环流特征也不相同，锋区对应的上升流特征与锋区表面通常观测到冷水现象吻合，锋区上层水体沿潮汐锋方向流速较强。另外，数值试验结果显示了地形和潮混合对潮汐锋的形成及锋区环流有重要影响。

关键词: 潮汐锋的三维流场, 潮混合, 地形